PUBLICATIONS OF THE ASTRONOMICAL SOCIETY OF THE PACIFIC, **113**:1232–1242, 2001 October

The Confusion Limit on Astrometry with the *Space Interferometry Mission*

JAYADEV RAJAGOPAL, TORSTEN BÖKER,[1] AND RONALD J. ALLEN

Space Telescope Science Institute, 3700 San Martin Drive, Baltimore, MD 21218; jayadev@stsci.edu, boeker@stsci.edu, rjallen@stsci.edu

Received 2001 June 4; accepted 2001 July 3; published 2001 September 4

ABSTRACT. An important requirement for the *Space Interferometry Mission* (*SIM*) is to carry out precision astrometry in crowded fields. This capability is crucial, for example, to accurately measure proper motions of bright stars in nearby galaxies. From such measurements, one can obtain distance estimates, explore the dynamics of these systems, and measure the mass of the Milky Way itself. In this paper, we investigate errors introduced by confusion, i.e., the presence of objects other than the targeted star in the *SIM* field of view (FOV). Using existing *Hubble Space Telescope* images of fields in M31, the LMC, and the Galaxy, we simulate the background within the *SIM* FOV and estimate the errors in the measured position of the target star. Our simulations account for the error contribution from photon statistics. We also study the effects of pointing imperfections when a field is revisited, which result in errors in the measured proper motion. We use the simulations to explore the measurement accuracy of several *SIM* key programs that will require crowded field astrometry. In M31, the error in the absolute position of the targets could be significant for all but the brightest targets. Our results also indicate that, in the case of the brightest targets in M31 and for all likely target magnitudes in the other cases, confusion-induced proper-motion errors are well within the *SIM* requirements. However, targets that vary in flux between measurements can be susceptible to enhanced proper-motion errors. We also find that, for an on-source integration time of 1 hr, photon noise is larger than or of comparable magnitude to the confusion-induced position error for bright targets and dominates over proper-motion error in most cases.

1. INTRODUCTION

The *Space Interferometry Mission* (*SIM*) will allow astrometric measurements that are several hundred times more accurate than currently possible at optical wavelengths (e.g., *Hipparcos*; Perryman et al. 1997). The key to this giant leap in precision lies in exploiting the remarkable wave front stability in space via optical interferometry. *SIM* promises to achieve microarcsecond accuracy for astrometry on objects as faint as $m_v \lesssim 20$. At these faint levels, the presence of even fainter stars inside the astrometric field of view (FOV) is likely to perturb the astrometric measurements. Such "confusion" errors could limit the astrometric accuracy achievable with *SIM*. Some examples for *SIM* key projects[2] that are likely to be affected by the presence of additional "background" objects are (1) the determination of distances and ages of globular clusters; (2) mass estimates for stars and dark objects such as stellar remnants, brown dwarfs, and planets via astrometric microlensing; and (3) dynamical studies of external galaxies.

In this paper, we explore the effects of confusion on typical *SIM* astrometric measurements. More specifically, we model a number of target fields that we expect to be typical for the above projects. These fields cover a fairly wide range in the degree of crowding, from the densely populated M31 disk through the moderately crowded LMC to a sparsely populated field in the bulge of our Galaxy. The results of this paper thus should be useful for most *SIM* key projects to gauge the effect of crowding on the astrometric accuracy of the respective measurements.

The term "confusion" is most commonly used in connection with the accurate measurement of target *amplitude* and has a rich history in the context of the determination of the "log *N*–log *S*" source count relation in radio astronomy and the application of radio source counts to cosmology.[3] Faint sources in the background that are within the FOV of the telescope (i.e., in the "beam") are a source of noise that does not reduce with further integration. Their contribution to the estimates of source amplitude has by now been thoroughly understood (Scheuer 1957; Condon 1974; Franceschini 1982). Confusion errors in astrometry from imaging surveys have also been a subject of interest of late (Hogg 2001).

In the case of astrometry with *SIM*, although the source of the noise is still faint background sources within the FOV, we are especially concerned with the effects of this confusion on the target *position*, taken in the context of an interferometric measurement of fringe phase. We investigate the role that in-

[1] Affiliated with the Astrophysics Division, Space Science Department, European Space Agency.

[2] For a summary of the recently selected *SIM* key projects, see http://sim.jpl.nasa.gov/ao_support/ ao_abstracts.html.

[3] Mills (1984) has given an interesting retrospective of the controversy between the Australian and Cambridge results on this subject in the 1950s.

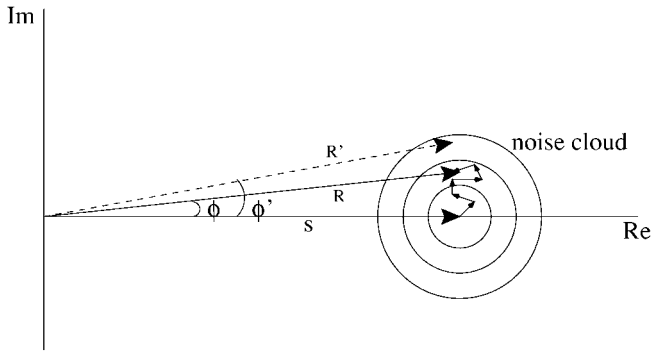

FIG. 1.—Schematic clarifying the phasor notation for our confusion model. The target phasor *S* lies along the real axis (reference phase set to zero). The random sum of the confusing sources (denoted by the small-amplitude phasors at the tip of *S*) perturbs the phase measurement for *S*. The resultant *R* has phase ϕ (the position error). On a subsequent visit to the same field, pointing errors can result in a slightly different phase (ϕ') for the resultant (R'), causing a proper-motion error.

strumental parameters such as the FOV, the system bandwidth, and the repeatability of the aperture repointing play in the confusion error. The prominent role that interferometric techniques are likely to play in future space-based astronomy serves as ample motivation for this study.

The primary advantage of astrometry from space over ground-based interferometric methods is that atmospheric turbulence is avoided. Space-based interferometers are essentially phase-stable instruments. Phase referencing within a fairly narrow FOV can be used to overcome some of the atmosphere-induced errors from the ground, but this is limited to narrow angle astrometry. Phase referencing using a star in the FOV also imposes sensitivity limits on ground-based interferometers. Low surface brightness or extended objects are difficult targets for fringe phase tracking from the ground. Space interferometry therefore offers a big advantage for wide-angle astrometry and can reach fainter objects than is possible from the ground. For example, the Navy Prototype Optical Interferometer (NPOI; Armstrong et al. 1998) will achieve milliarcsecond accuracy for wide-angle astrometry from the ground using 35 cm apertures and baseline lengths of 19–38 m. *SIM* promises microarcsecond accuracy with similar aperture sizes and shorter baselines (up to ~12 m). The limiting magnitude for NPOI is expected to be of the order of $m_v = 7$ as compared with the *SIM* limiting magnitude of $m_v \approx 20$.

A tutorial covering the basics of astrometry with *SIM* can be found in Shao & Baron (1999). Briefly, *SIM* uses interferometry to measure the angle between two stars. The position of a delay line that results in a "white-light" or zero–path-difference fringe is measured to a precision of ≈0.1 nm (corresponding to a few microarcseconds in the sky) on a *reference* star. The basic astrometric observable is the relative position of the delay line with respect to this "fiducial" when a white-light fringe is obtained on the *target* star. This measurement can directly be translated to an angle in the sky between the two objects, projected perpendicular to the baseline orientation. The measurement is done for two mutually perpendicular orientations of the *SIM* baseline, thereby yielding the true angle between the reference and target sources. The orientation of the baseline in a reference frame is determined by observing selected "grid" stars, and "guide" stars are used to maintain the attitude of the spacecraft to the high accuracy required.

Finding the position of the delay line for a white-light fringe is the basis of astrometry with *SIM*. This in turn involves measuring the phase or position of the fringe pattern accurately. At least three sources of error can occur: (1) the source structure itself can change over the course of a measurement or between measurements; (2) objects in the FOV other than the target star can add to the fringe pattern, which leads to a modified fringe phase and thus to errors in the measured position of the star; and (3) errors in the pointing of the siderostats can alter the FOV (for repeated visits to the target) and hence the background sources included in the FOV. This causes errors in the measured relative position of the target between visits, which reflects as a proper-motion error. In this paper, we address the latter two sources of error in detail. We also comment briefly on the first source of error, namely, proper-motion error induced by the source varying in flux, a situation that might be of concern, e.g., in microlensing studies.

In § 2 we present an analytical approach that provides a simple mathematical description for confusion errors and a way of arriving at a first estimate for the magnitude and scaling for such errors. Section 3 describes the various steps involved in the numerical simulations we have carried out to determine these errors accurately. We present the results of these simulations for the specific fields we have considered in §§ 4 and 5. Section 6 is a brief summary.

2. CONFUSION ERRORS IN INTERFEROMETRIC ASTROMETRY

Confusion in the present context is the error introduced into the fringe phase of a fairly strong signal (the target star) when superposed on a set of fringes from weaker, randomly distributed sources (the background stars in the FOV). Phasor notation is well suited to depict the fringe amplitude and phase (the complex-valued fringe visibility) in this case (e.g., Ryle 1959). The errors in the measured fringe phase for a *SIM* astrometric measurement in a crowded field can be derived from the well-defined statistical properties of the sum of a strong constant phasor plus a weak random phasor sum (Goodman 1985). A schematic representation is given in Figure 1. For a noiseless measurement, the fringe visibility of a source at the phase center of the FOV is represented by a phasor of amplitude *S* and phase zero,[4] i.e., lying on the real axis. Background sources perturb the fringe phase and are represented by the small-amplitude,

[4] This is the reference phase and can be set to zero without loss of generality.

random-phase phasors at the tip of the strong phasor. The loci (for different realizations) of the tip of the phasor sum of the background are the circles that form a noise "cloud." The phase of the resultant R is now ϕ. The interferometric fringe phase ϕ for a given baseline B and wavelength λ is given by

$$\phi = \frac{2\pi B \sin\theta}{\lambda}, \quad (1)$$

where θ is the angular distance of the source from the line perpendicular to the baseline orientation. It follows that the rms value for ϕ represents the error in phase and hence in the measured position (θ) of the target. In the case of background sources that are weak compared with the target star, it can be seen from Figure 1 that ϕ is primarily decided by the imaginary part, Im (R), of the random phasor sum. On a subsequent visit to the field, a slightly different set of background sources contribute to the random sum because of pointing errors, and the total resultant is now denoted by the dotted line (R'), with a phase ϕ'. The difference $\phi' - \phi$ represents the error in measured proper motion between the two visits. Here again it is the imaginary part of the difference between the random sums, Im ($R' - R$), which dominates the error.

The position and proper-motion error caused by confusion alone can be analytically estimated from the statistics of the random phasor sum involved. We can estimate the standard deviation of the phase (in Fig. 1) of a fringe produced by the target star from

$$\sigma(\phi) = \sqrt{\Sigma(X_i)^2/(2S^2)} \text{ rad}, \quad (2)$$

where X_i are the intensities of the background sources (the amplitudes of the weak random phasors) and S is the target star intensity (the strong constant phasor; Goodman 1985). This quantity is the confusion error in the position of a source in a crowded field. The error in proper motion ($\phi' - \phi$ in Fig. 1) due to pointing inaccuracies is given by the ratio Im($R' - R$)/S and scales inversely as the target intensity. Equation (2) shows that the position error $\sigma(\phi)$ also scales inversely with the target intensity S.

The above description provides a simplified picture for the nature of confusion in interferometric astrometry. In practice, the situation is more complicated because of photon noise contributions and effects of the finite bandwidth. The finite bandwidth efffectively reduces the FOV. Sources at larger angular distances from the line perpendicular to the baseline orientation suffer larger decoherence. To clarify, recall that equation (1) gives the interferometric phase for a single wavelength λ. For a finite band, the amplitude of each of the random phasors in Figure 1 results from vector-adding all the phasors corresponding to each wavelength in the band. This results in a reduction of the amplitude, an effect that is larger for phasors with larger phase angles, i.e., sources at larger distances from zero delay. In essence, this is the "delay beam," which progressively decreases the contribution of background sources to the resultant fringe as they are moved farther away from the line perpendicular to the baseline orientation. In order to account for these effects, we have simulated typical *SIM* fields and numerically estimated the total astrometry error from confusion and photon noise with bandwidth decorrelation taken into consideration. In the absence of detailed information on detector characteristics, we have not modeled read noise or other similar sources of error. The rest of this paper describes these simulations and their results. In an earlier study, we have estimated both position and proper-motion errors using the statistical results described above for the specific example of M31 (Rajagopal, Allen, & Böker 1999). The earlier results are consistent with those achieved with the full simulation described here.

3. THE SIMULATIONS

A prerequisite for estimating errors from confusion effects is to build a model of the sky as seen at the *SIM* resolution. Our model of the background seen in a typical *SIM* FOV is based on *Hubble Space Telescope* archival images taken through the Wide Field Planetary Camera 2 (WFPC2). The resolution afforded by the *HST* images is important to model the changes in the background structure accurately for *SIM* pointing errors, which are of the order of a few tens of milliarcseconds. In this section, we detail the steps involved in the simulation. We account for the effects of the point-spread function (PSF) of the siderostats, size of the field stop, and the bandwidth used. We chose the fields to be typical examples for the kind of targets that *SIM* is likely to study extensively, and we discuss each example in detail in §§ 4 and 5.

The simulation involves the following basic procedure.

1. In approximating the *SIM* FOV, we assume that the astrometry measurements are carried out using a baseline of 10 m. Using the *HST* image to constrain the total flux in the *SIM* FOV, a model sky field at the resolution afforded by this baseline (~10 mas at a wavelength of 600 nm) is constructed. An area large enough to accommodate the effective *SIM* FOV is chosen at random on the *HST* image. The simulated FOV is constructed with 5 mas pixels (assuming Nyquist sampling for *SIM*), and the total flux is redistributed in this field among stars randomly drawn from a luminosity function (LF). For all our sample fields, we have used the LF for the solar neighborhood from Yoshii, Ishida, & Stobie (1987) with appropriate limits, which are specified in the discussion for each field. Each star is then put down as a δ function at random positions within that FOV. The *SIM* astrometry measurement is simulated for a number of such locations.

2. Once the background has been modeled as seen at *SIM* resolution, the next step involves calculating how each of these sources contributes to the measured fringe amplitude and phase. There are three parameters that define the relative strengths of their contributions: the PSF of the individual *SIM* siderostats, the size of the field stop in the optical path, and the bandwidth decorrelation effect. While the first two affect the total number of photons available from a source depending on its position

in the FOV, the third modulates the coherence of the light from a source, thereby affecting its contribution to the fringe pattern without changing its photon flux. To account for the siderostat PSF and the field stop, we multiply the FOV by a function obtained from the convolution of the Airy disk (at the center wavelength) of the siderostats with the field stop function. This function is centered on the FOV. The actual area of the image considered is greater than the FOV to account for contributions from sources beyond the edges of the field that "leak" in because of diffraction effects. The PSF is calculated for a siderostat diameter of 30 cm (the currently expected size for the *SIM* apertures). The field stop shape has as yet not been decided, and we have assumed a square stop.

3. We discuss the effects of bandwidth decorrelation (the delay beam) for bands of 12 and 400 nm centered at the WFPC2 filter center. The expected total bandpass for *SIM* is ~400 nm (from 500 to 900 nm), with the fringes dispersed into individual channels of width ~6 nm. Hence, the lower value we have used is appropriate for summing two channels, whereas the higher one is applicable when most of the channels are coadded. Binning channels to estimate the fringe phase is done postobservation, and these two cases correspond to the two limits for the number of channels added together. The location of the center of the delay beam on the sky is decided by the positioning of the delay line. The nominal value for the error in delay line position is ~10 nm, which corresponds to roughly 2% of the fringe width at the shortest wavelength. We neglect this source of error in the simulations; i.e., the position of the delay beam is considered stable and only the FOV is "jittered" to account for pointing errors. The delay beam corresponds to a strip in the sky perpendicular to the given baseline orientation. Its profile is given by the Fourier transform of the bandpass function. Here we assume a rectangular bandpass. The decorrelation is implemented by simply vector averaging the visibility values at the (u, v) coordinates corresponding to the 10 m baseline at the center wavelength of each channel in the band considered. The effect of the finite channel width is ignored.

4. Finally, we account for the photon noise contribution to the errors. This is done by simulating the fringe visibility measurement as described in Böker & Allen (1999). In brief, the delay line is stepped through four different values of delay around the white-light or zero–path-length difference setting. The photon counts in each of the four delay bins for each channel are then used to calculate the fringe visibility. This procedure is simulated for typical bandwidths and integration times and the counts in each bin modified according to Poisson statistics to account for the photon noise. To obtain estimates for confusion noise alone, this feature can be switched off.

5. The preceding steps allow us to "measure" the fringe phase corrupted by both confusion from other objects in the FOV and photon noise. To arrive at the fringe phase, we Fourier transform the simulated FOV and pick out the phase of the Fourier component corresponding to the baseline used (10 m).

6. To calculate the rms error in the measured position of a target star, we determine the fringe phase of the target star, which is introduced into the FOV at the phase center (and therefore expected to have zero phase). By simulating the measurement at a number of different locations (100 in this case) on the image and measuring the spread of values for the measured phase, we can estimate this error. In the absence of photon noise, this corresponds to the position error for the target because of confusion from background objects.

7. For a proper-motion measurement, the same field is visited more than once and changes in the position of the target are measured. For each visit, the FOV will be slightly different because of pointing errors. The relative change in the phase of the measured fringe (because of the different distribution of background sources) manifests as an error in the measured proper motion. To simulate this error, steps 1–4 are done, and the *change* in phase ($\Delta\phi$) of the 10 m Fourier component as the FOV is shifted by a small amount is measured. This is repeated at each location for a range of values for the pointing error, and the spread in the values of $\Delta\phi$ is computed as the estimate for error in proper motion because of pointing errors in a crowded field. The shifts are carried out in the direction perpendicular to the delay beam orientation. This is the direction in which the maximum change in background is expected and provides a worst-case estimate of confusion-induced proper-motion errors.

3.1. Important Instrument Parameters

The important instrument parameters that we assume for the simulations are:

Baseline length.—We have used a baseline length of 10 m for all results quoted here.

Mirror size.—The siderostat diameter assumed is 30 cm.

Throughput.—We have assumed an overall throughput of 0.3.

Field stop size.—The field stop diameter (or side for a square stop) is expected to be in the range of 0.″3 (the FWHM of the PSF at 600 nm) to 1.″0.

Bandwidth.—*SIM* is expected to have a wavelength range of 400–900 nm, with a resolution of ~6 nm. We specify the bandwidth used for each example presented here.

Pointing accuracy.—On a bright source, where the star trackers can be used to guide the instrument, the pointing accuracy is expected to be of the order of 10 mas. This is the accuracy to which a given pointing can be repeated. The jitter on any individual pointing will be less than this value. For a faint source, the instrument will make use of information from the guide interferometers to maintain pointing. In this case, the accuracy for revisiting the field is expected to be ~30 mas. We show results for a range of pointing offsets.

In the case of the M31 field, we performed the simulations using a range of likely values for some of the crucial design parameters for *SIM* that are either not yet fully specified or are likely to vary depending on the observation strategy chosen. These include the bandwidth, the field stop size, and the point-

ing accuracy, and we have attempted to establish the trends in astrometry error for different values of these. In the case of the LMC and Galactic bulge fields, we show results for a given set of the most probable values for these parameters.

4. RESULTS FOR M31

We used archival *HST* images (Program ID 5971, PI: R. E. Griffiths) of a region of the M31 disk taken with the WFPC2 through the F606W filter (mean wavelength ~584 nm) to model the background seen by *SIM*. We have chosen this field (Figs. 2 and 3) to be located in the disk of the galaxy in an area where a typical astrometry measurement for measuring "rotational parallax" might be carried out. Measuring the distance to M31 using this method is an idea that dates back to the beginning of the century. It involves obtaining the proper motions of individual stars in the disk at several locations. When combined with radial velocity measurements, this yields an independent estimate of the distance to the galaxy, as well as its rotation curve and inclination to the line of sight. For the first time, *SIM* will provide the necessary precision to achieve these remarkable goals. The required accuracy of proper motion is of the order of 5 μas yr^{-1} for stars of magnitude $m_v = 16$ in the M31 disk (Olling & Peterson 2000), which is within reach of the sensitivity limits specified for the mission (Allen, Peterson, & Shao 1997).[5] However, in the case of crowded fields, the effect of confusion needs to be studied in detail and will have an important role in defining the actual limits of astrometric precision.

4.1. Source Model

The image is from co-added multiple exposures and has a net exposure time of 5600 s. It has been subjected to the pipeline calibration procedure. The multiple exposures have been used to remove cosmic-ray events. The resolution is ~0.″1 pixel^{-1}. Each of the three WFPC2 chips covers ~80″ of the sky.

To model the FOV at *SIM* resolution (step 1 of previous section), we use the LF for the solar neighborhood from Yoshii et al. (1987). This LF has been extrapolated at the high-luminosity end to an absolute magnitude (*V* band) of -8.5. The linear extrapolation uses a logarithmic slope of -5.4, which is consistent with the measured slope of the LF in the relevant magnitude range in M31 (Hodge, Lee, & Mateo 1988). The high-end limit corresponds to an apparent magnitude of 16 at the distance to M31 (distance modulus of 24.5; Stanek & Garnavich 1998), which is the proposed typical magnitude of a target star for the rotational parallax observations. For the low-luminosity limit, we use an absolute *V* magnitude of 6.0 ($m_v = 30.5$), which is well below the expected *SIM* sensitivity limit of $m_v = 20.0$ (Allen et al. 1997). The integrated flux flattens out at this magnitude, indicating that the flux contribution from fainter stars is negligible.

For this field as well as all other simulations described in this paper, we have investigated the error in both position and proper motion. Two important parameters that influence the magnitude of these errors are the extent of the FOV and the effective bandwidth used. We have varied these parameters to gauge their influence on the accuracy of astrometric measurements with *SIM*. This will be relevant for both the *SIM* design and observing strategies adopted.

4.2. Position Error

We briefly describe here the results of our simulation on the M31 field to gauge position error (see Table 1). Here and in the following sections, we quote errors for the assumed baseline of 10 m and wavelength of 600 nm. The target star in our simulation is at the phase center and in the absence of noise should have a measured fringe phase of zero. For a bandwidth of 400 nm (from 500 to 900 nm) and a field stop size of 1″, the rms deviation from this value because of background sources alone (no photon noise) is of the order of 0.7 μas for a target star of $m_v = 16$ and is a measure of the position error. A narrowband (12 nm) case shows a significant increase in the position error since the bandwidth decorrelation is now much reduced (the delay beam is now much broader) and a larger number of confusing sources contribute to the error phasor. The number of contributing sources is now limited by the size of the field stop. We find that the error is reduced by a factor of 2 when the field stop size is decreased to 0.″3. In some trials, the (weighted) FOV includes sources that are of comparable magnitude to the target and lead to comparatively large errors. Identifying these outliers through fringe-fitting (Dalal & Griest 2001 discuss fringe-fitting for some specific examples of LMC fields) or avoiding such fields through preselection can cause the error to be reduced by a factor of 3 or more as discussed in more detail in the following section. The errors scale approximately as the inverse of the flux ratio (see Fig. 7), in agreement with the analytic expression for confusion error in § 2. It is evident from Table 1 that position errors are quite significant when compared to the required *SIM* accuracies for all except the very brightest targets.

4.3. Proper-Motion Error

The results for the proper-motion error are also summarized in Table 1. Figure 4 shows the proper-motion error for a range of pointing offsets for a 16th magnitude target star. These are estimated as described in § 2 (step 7) by taking the standard deviation of the change in phase for a given pointing offset over a number of randomly picked locations on the *HST* image. The simulations do not include photon noise, and the error is from confusing sources alone. Figure 4 is for a bandwidth of 400 nm (from 500 to 900 nm), which covers most of the *SIM* spectral range, and the field stop is a square of side 1″. Here the large

[5] For *SIM* science requirements, see also the report of the *SIM* Science Working Group at http://sim.jpl.nasa.gov/library/technical_papers.html.

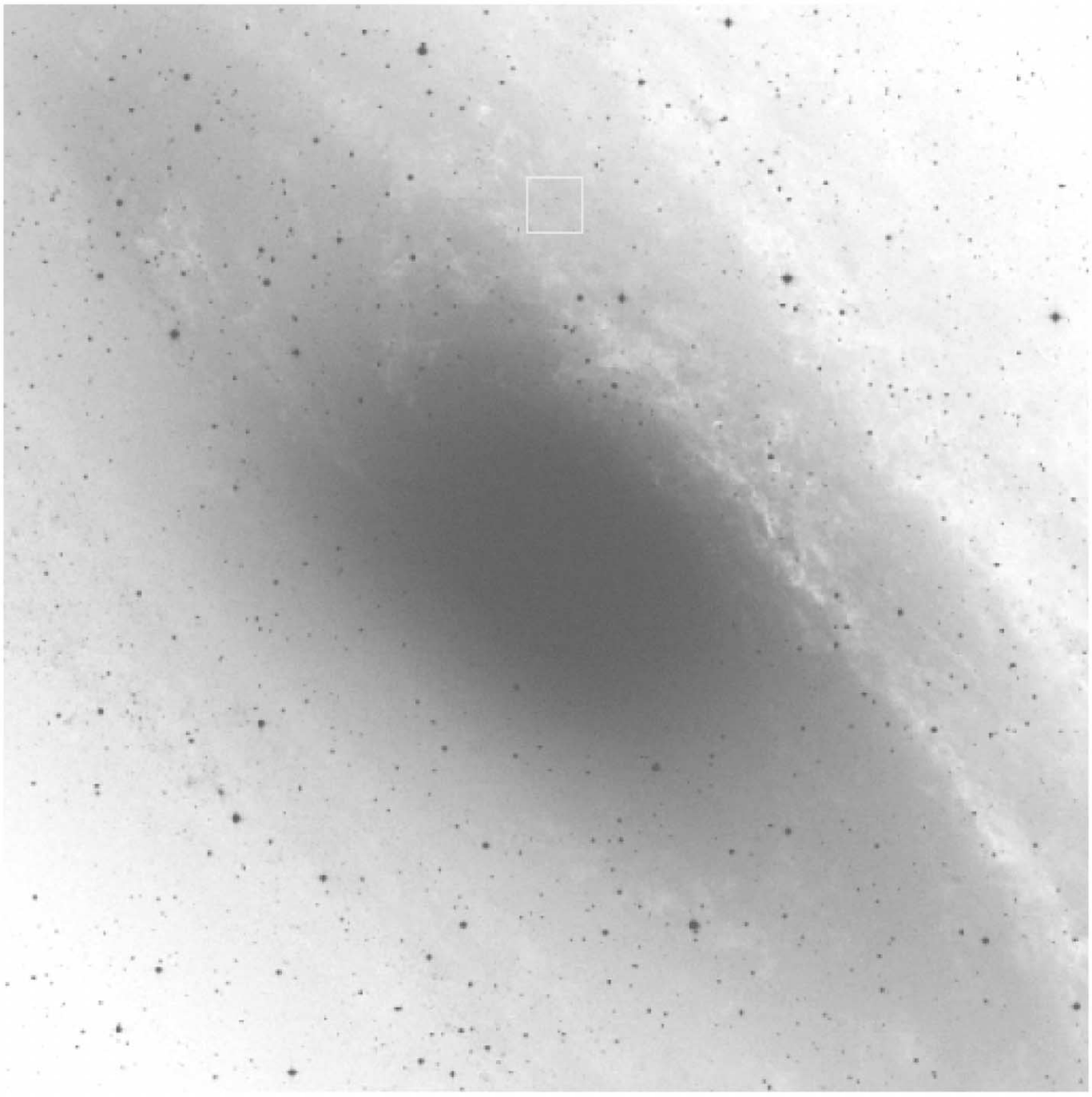

FIG. 2.—Digitized Sky Survey image of M31 (30′ × 30′). A typical location chosen for our simulations is marked.

bandwidth decorrelation effect dominates in deciding the effective FOV and the confusion. The value for proper-motion error at 0.″01 pointing offset is ~0.006 μas. This is negligible compared with the specified instrument accuracy of ~1 μas and the required proper-motion accuracy of ~5 μas for the rotational parallax experiment (Olling & Peterson 2000). Figure 5 (*triangles*) is for a bandwidth of 12 nm (694–712 nm). The proper-motion errors have increased by a factor of ~10, still small compared with the sensitivity required. The error increases since the bandwidth decorrelation is reduced and more sources contribute to the confusion. Since the delay beam does not dominate (unlike in the broadband case) in limiting the extent of the effective FOV, the weighting function derived from the Airy disk and field stop size (step 5 in § 2) may play a role in the magnitude of

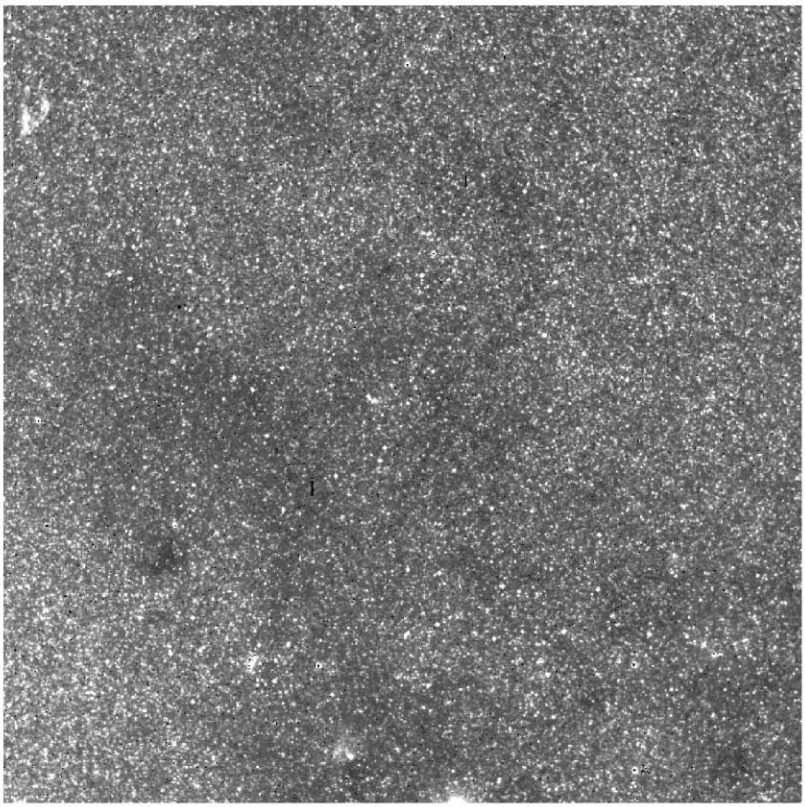

FIG. 3.—WFPC2 image of the location in the M31 disk shown in Fig. 2, approximately 1′ to the north of the nucleus (F606W filter, ~70″ × 70″ with 0.″1 pixel^{-1}). Several stars of $m_v = 16$ have been introduced to help gauge the relative background surface brightness.

the confusion error. In Figure 5, we also show the results when the field stop size is decreased to 0.″3. We do not find a significant change in the proper-motion error. This is different from the position error, which did decrease with stop size. The field stop size therefore can be chosen to maximize the throughput because confusion is unlikely to play a role in this design criterion.

The large position errors in Table 1 do not result in large *proper-motion* errors since most of the position error is common between visits and therefore cancels out. However, if the target flux were to change between visits, the position errors (which scale inversely as the target flux) would not cancel out and would indeed cause proper-motion errors. A typical example would be a proper-motion measurement for a microlensing event, where the brightness of the lensed object can easily change by 1 mag or more. For a 19th magnitude target in the LMC, the position error is ≈3 μas (§ 5). If the target dims to 20th magnitude on a subsequent visit, the position error scales to ≈7.5 μas. The difference or "proper motion" measured would therefore be 4.5 μas from this effect alone. In comparison, the typical signal in such experiments would be only a few microarcseconds. We note the serious nature of this problem here and hope to address possible remedies in a future publication.

TABLE 1
SUMMARY OF RESULTS FOR M31

BANDWIDTH (nm)	FIELD STOP (arcsec)	POSITION ERROR (μas)		PROPER-MOTION ERROR (μas)	
		$m_v = 16$	$m_v = 19$	$m_v = 16$	$m_v = 19$
400	1.0	0.7	9.9	0.01	0.1
12	1.0	3.2	53.1	0.06	0.9
12	0.3	1.9	30.0	0.05	0.8

NOTE.—The proper-motion errors are for a pointing offset of 0.″01, the value adopted as the nominal pointing error for the *SIM* siderostats. The phase errors in radians have been converted to angle in the sky using a baseline of 10 m, for a central wavelength of 600 nm. No photon noise is included. Note that the errors scale inversely with target flux.

Figure 6 shows a histogram of the error in proper motion measured with a 10 m baseline for a 16th magnitude target star as the FOV is offset by 0.″01 (the pointing error) at 100 random locations in the *HST* image. The histogram has a central peak and some outliers. These large deviations in phase are a result of background stars of comparable magnitude to the target in some of the locations, and these contribute significantly to the standard deviation of the samples and hence to

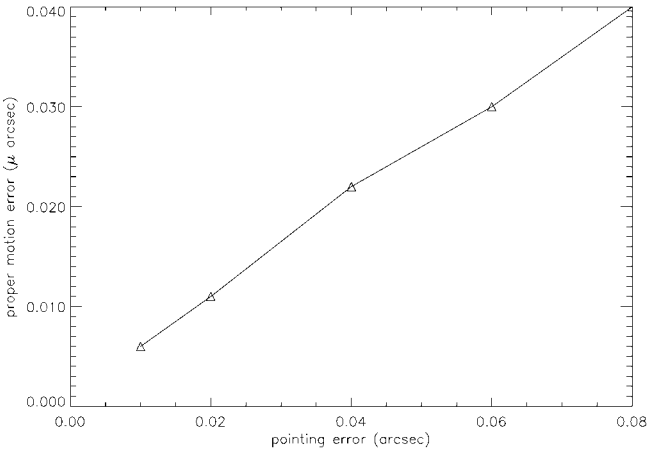

FIG. 4.—Proper-motion error due to confusion vs. pointing offset for the M31 field, for an $m_v = 16$ target star. The bandwidth used is 400 nm, and field stop size is 1″. The pointing accuracy for *SIM* is expected to be ~0.″01. The proper-motion error for other values of target brightness can be obtained by scaling inversely as the target flux.

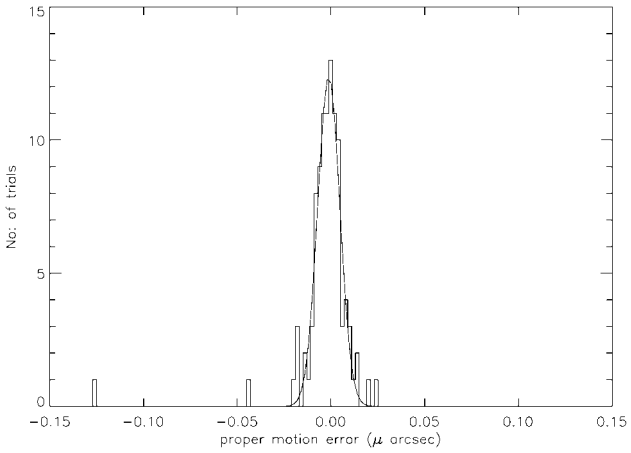

FIG. 6.—Histogram of the error in proper motion for the M31 field for 100 trials using a pointing offset of 0.″01, with other parameters the same as in Fig. 4. The width of the distribution is a measure of the proper-motion error. The Gaussian fit to the central peak is shown.

the error estimates. It is likely that careful selection of *SIM* target fields will avoid this problem. We show in Figure 6 a Gaussian fit to the central peak of the distribution to estimate the proper-motion error (the σ of the Gaussian). All values for both position and proper-motion errors listed in this paper are derived in this fashion. The directly computed standard deviation is a factor 3–5 greater than these values because of the outliers. However, the scaling of the errors with target star magnitudes or pointing errors is not affected.

4.4. Scaling with Target Flux

From equation (2), both the position and proper-motion errors are expected to scale inversely with target brightness. In Table 1 we show the error values for targets of $m_v = 16$ and 19 to demonstrate this. In addition, Figure 7 shows the scaling of both astrometry and proper-motion errors with the inverse flux ratio, normalized to the value for a target star of $m_v = 16$ and a bandwidth of 400 nm. The scaling is approximately linear until the target flux drops by a factor of ~15 ($m_v = 19$). The simulations show that as the target flux drops beyond this value the confusion error starts to flatten out as the "noise cloud" (Fig. 1) starts to be of comparable amplitude to the target phasor itself. In this limit, the linear scaling law is no longer applicable. Figure 8 shows the scaling of the proper-motion error with magnitude for the 12 nm bandwidth case. The scaling is shown for field stop sizes of 1.″0 and 0.″3. Here also the scaling is linear for moderate flux ratios.

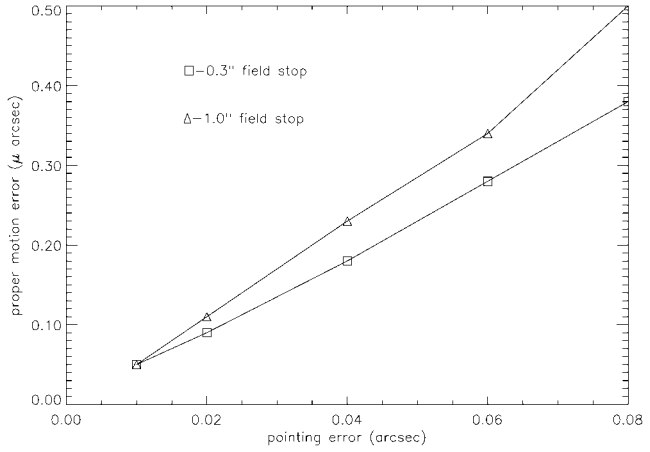

FIG. 5.—Proper-motion error for the M31 field, with parameters the same as in Fig. 4 except for the bandwidth, which is now 12 nm.

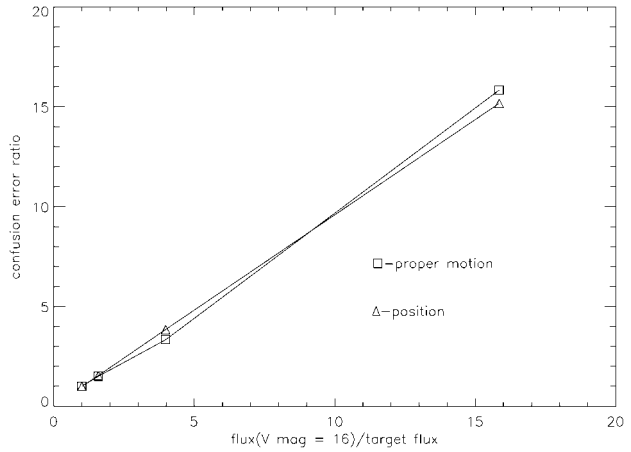

FIG. 7.—Scaling of confusion errors with target flux (broadband). The squares show the proper-motion error ratio (normalized to that for a target with $m_v = 16$), and the triangles are for position error. Both errors scale inversely as the flux. The bandwidth used is 400 nm, and field stop size is 1″.

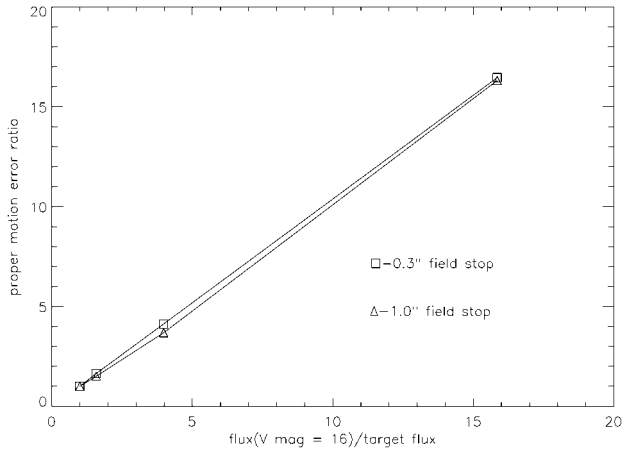

FIG. 8.—Scaling of confusion errors with target flux (narrowband). The triangles show the proper-motion error for a bandwidth of 12 nm and field stop size of 1″. The squares are for a stop size of 0.″3.

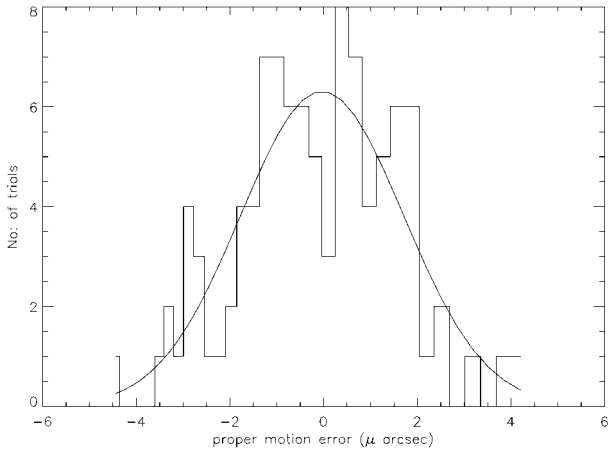

FIG. 9.—Histogram of proper-motion errors with photon noise included. All other parameters are the same as in Fig. 4. The Gaussian fit shown has a σ of 2.0 μas. Clearly, photon noise dominates over confusion (cf. Fig. 6) for this case.

4.5. Photon Noise

We show in Figure 9 the proper-motion error histogram from a simulation with photon noise contribution included. The input parameters are the same as in Figure 6 (which does not have photon noise), with an integration time of 1 hr. The photon noise clearly dominates the error in measured phase and is a few hundred times larger than the confusion-induced proper-motion error. For the case shown, the measured phase distribution has a σ of ~0.001 rad, which implies an error in the measured proper motion of ~2.0 μas (as in all cases, this is for a baseline of 10 m and central wavelength 600 nm). The size of the field stop plays a role in the photon noise contribution. A stop of diameter 1″ allows 80%–90% of the target flux through for the 500–900 nm wavelength range and a 30 cm aperture. Further increase of the stop size will increase the background flux level without adding significantly to the source flux, and the fringe visibility is reduced. This directly increases the phase error as

$$\phi_{\rm rms} = \frac{C}{2\pi V\sqrt{N}},$$

where C is a constant, N the photon number, and V the fringe visibility (Shao & Staelin 1977). However, for the cases we have studied, the target flux is high enough that the background contributes only a small fraction of the overall flux, and hence this effect is well below the statistical errors in our simulations.

The magnitude of the error in the measured absolute position of the target from photon noise is similar to that in the above case. Hence, it is clear that the confusion-induced position error (see Table 1) is of comparable magnitude to the photon noise error for the brightest targets in M31. Since confusion error scales inversely as the flux and the photon noise scales inversely as the square root of the flux, the position error can be dominated by confusion for weaker targets.

4.6. Some Approximations

Before presenting the results for the other fields, we discuss some important approximations assumed in the simulations and possible consequences.

In principle, the estimates of noise from confusing sources could be affected by the photon noise in the *HST* image we use to model a *SIM* FOV. Since we attribute all the flux to point sources, photon noise–induced variations can introduce false structure into the simulation. However, the typical pixel-to-pixel variance measured in the deep exposure images of the M31 disk that we use are 8–9 times larger than expected from Poisson fluctuations of the photon counts, so the structure in the image is real. The formal errors (1 σ) on the Gaussian fits (with statistical weighting for the bin counts) to the phase deviations are ~10%. The formal errors are consistent with the variations between different runs of the simulation. We therefore take this value as the error in our estimates for confusion noise. We note that eliminating fields with bright background sources can systematically reduce the error.

We model the position offset (caused by pointing errors) to be perpendicular to the orientation of the delay beam on the sky, in order fully to gauge the effect of the bandwidth on the confusion error. For the wideband (400 nm) case, this is likely to give larger estimates for the confusion than in the actual case of pointing offsets in random directions. For the narrow band, the bandwidth decorrelation has minimal effect irrespective of the adopted direction for pointing offsets.

The only instrumental errors we have considered for this analysis are pointing imperfections. In the absence of detailed

information of other systematic errors, we currently believe that pointing is indeed the major factor for confusion issues.

5. RESULTS FOR THE LMC AND THE GALACTIC BULGE

The magnitude of confusion errors in *SIM* astrometric measurements is clearly affected by many factors. For example, the distance to the target field and the structure of the background play important roles. For this reason, it is difficult to extend the M31 results to other fields in any simple fashion. To gauge the effect of distance to the target field on the confusion problem, we carried out simulations on typical fields in the LMC and our own Galaxy. Together, these three cases form a fairly representative sample of distance, surface brightness, and the degree of crowding for most targets that *SIM* is likely to observe. Hence, these results are useful in estimating the extent of confusion for most *SIM* programs. The main results are described below for comparison with the M31 results.

Fields in both the LMC and the Galaxy will be observed by *SIM* for a variety of reasons. For example, the fields we have chosen are typical candidates for microlensing events. The lensing event causes a shift in position of the centroid of the lensed star. This shift along with the measured light curve can be used to obtain distances to the lensing and lensed object as well as the mass of the lens. These experiments try to detect a relative change in position of the target star over repeated visits to the field. The presence of other sources in the FOV, coupled with pointing inaccuracies, causes proper-motion error. For both the LMC and bulge microlensing events, the predicted centroid shift is of the order of a few microarcseconds. In both cases, we have adopted a V magnitude of 19 for the target star. Since this is a fairly weak target (the *SIM* sensitivity limit is $\sim m_v = 20$), the experiment will aim to maximize the signal from the target. We therefore use a wide band (400 nm) and a field stop size of 1″ for these simulations. Here we aim to estimate the confusion noise alone and do not include the photon noise contribution. We have already demonstrated that, even in one of the more extreme cases of crowding (the M31 disk), photon noise is larger than the confusion-induced position error and dominates the proper-motion error for a 1 hr integration. Hence, the photon noise contribution to astrometry errors in the LMC and the Galaxy (or indeed any other field) can be scaled from that result using the total flux and standard Poisson statistics, neglecting the contribution from confusion.

Figure 10 shows the proper-motion error histogram for the case of the LMC field and a pointing error of 0.″01. The *HST* image (Program ID 5901, PI: K. Cook) used here is from the Planetary Camera (PC), with the F814W filter (I band) and 500 s exposure time. We use the same LF to populate the simulated *SIM* FOV as in the previous case, with upper and lower limits of $M_v = -1.0$ and 15, respectively. The histogram clearly shows that the proper-motion error has large excursions from zero for a few trials. As in the M31 case, this is due to

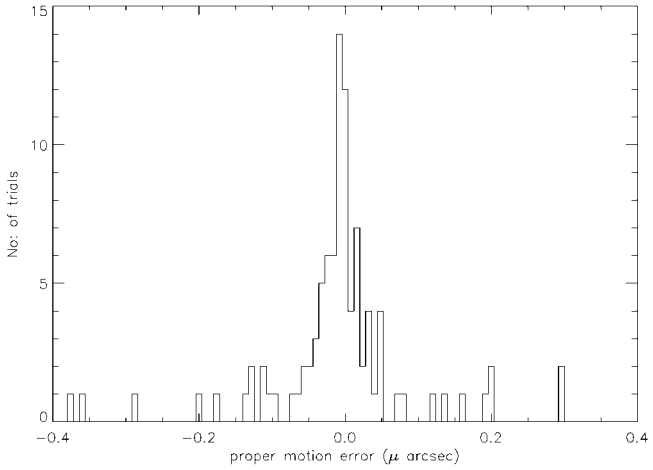

FIG. 10.—Histogram of proper-motion error from confusion for the LMC field. Compared with Fig. 6 (M31 field), the width of the distribution is narrow, indicating negligible confusion error. The outliers occur when a comparatively bright source other than the target is present in the FOV.

background stars of comparable magnitude to the target inside the FOV. Since the target magnitude of $m_v = 19$ ($M_v = 0.5$ for a distance modulus of 18.5 for the LMC; Madore & Freedman 1998) is much weaker than for the M31 case, the relative strength of the background sources within the FOV is higher, resulting in large deviations of the measured phase. Such fields should be easy to identify, and this effect can be accounted for (e.g., with fringe-fitting methods) to reduce the error. If we neglect the outliers in the histogram, the proper-motion error is negligible (0.02–0.03 μas). The position error for this case is ~ 3 μas. As described in § 4, this could be of significance in the proper-motion measurement if the target were to vary in flux.

For the Galactic bulge, we have used an *HST* PC image (Program ID 7437, PI: D. Bennet), taken with the F555W filter (V band) and a short exposure time of 40 s. In this case, photon noise in the *HST* image could affect the simulated background. To minimize this, we have used only those *HST* pixels with counts more than twice the rms noise level in the image. The LF used has limiting absolute magnitudes of 3.5 and 15.5. The target star has an apparent magnitude of 19 (the distance modulus used here is 14.6; Alves 2000). Other parameters are the same as in the LMC case. Figure 11 shows the proper-motion error histogram. Here also, except for instances of clear outliers, the proper-motion error is negligible and of the order of 0.002 μas. The position error in this case is ~ 0.2 μas.

6. SUMMARY

We have estimated the error in measured position and proper motion arising from sources other than the target in the *SIM* FOV and the dependence of this error on parameters such as pointing accuracy and target flux. We have also discussed the effect of the bandwidth and field stop size on this error.

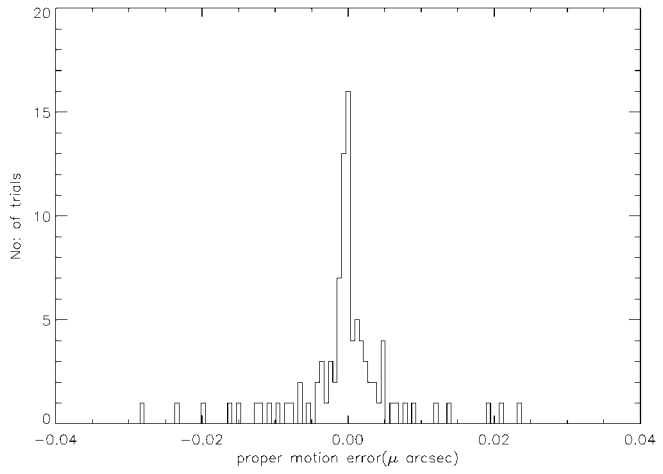

FIG. 11.—Same as Fig. 10 but for a Galactic bulge field. As in the LMC field, the distribution is quite narrow except for a number of outliers.

The error in position of the target star because of background sources is of the order of 1 μas for the M31 disk for the brightest possible targets. The error increases linearly with decreasing target flux. As is evident from Table 1, the position error is considerable for the narrowband case and is quite significant for weaker targets in M31. The same holds for the LMC and Galactic bulge as well.

Errors in proper motion are much smaller than the absolute position errors. This is because proper motion is essentially a relative measurement, and most of the confusion-induced position offset tends to cancel out between successive visits to the target. For the case of a target star of apparent magnitude $m_v = 16$ in the M31 disk, the proper-motion error is a small fraction of the required sensitivity for reasonable values of the relevant parameters. The target here is among the intrinsically brightest ($M_v = -8.5$) known stars. We show that the confusion-induced errors scale inversely as target flux, and the proper-motion error can be significant for weaker targets in M31. For the LMC and Galactic bulge, the confusion-induced proper-motion error is not a significant source of error even for targets close to the sensitivity limits specified for *SIM* (when using most of the available bandwidth). However, the fringe phase can be corrupted by the occasional strong source within the FOV. For the case of variable targets, the confusion-induced position offsets will not be the same between visits and hence will not cancel out in a proper-motion measurement. This could lead to large proper-motion errors, comparable to the position errors themselves.

For both position and proper-motion errors, significant reductions can be obtained by selecting fields without other objects of comparable brightness, identifying and removing the contribution to the fringe phase from such objects, and using all the available bandwidth for estimating the fringe phase.

The field stop size plays only a minor role for position errors in the wideband case since the narrow delay beam essentially limits the FOV. For the narrowband case, there is a decrease in confusion-induced position errors with decreasing field stop size. However, these errors are still within tolerable limits for bright sources for a field stop as large as 1″. A field stop of this size also maximizes throughput from the source without including too many background photons (in any case, for our sample fields the photon noise contribution from the background is small). We find that confusion-induced proper-motion errors are largely insensitive to field stop size.

The contribution from confusion to proper-motion errors is in most cases much less than that from photon noise for an integration time of 1 hr. The position errors from confusion, however, are of comparable magnitude to the photon noise and can even dominate for some cases.

We thank Ken Freeman, Dean Peterson, Steve Unwin, Roeland van der Marel, and Neal Dalal for discussions and suggestions. Rosa Gonzalez and Kailash Sahu helped us by providing access to and information about the *HST* archival images used in the simulations. The work described here was carried out at STScI with financial support from the *SIM* project at the Jet Propulsion Laboratory.

REFERENCES

Allen, R. J., Peterson, D., & Shao, M. 1997, Proc. SPIE, 2871, 504
Alves, D. 2000, ApJ, 539, 732
Armstrong, J. T., et al. 1998, ApJ, 496, 550
Böker, T., & Allen, R. J. 1999, ApJS, 125, 123
Condon, J. J. 1974, ApJ, 188, 279
Dalal, N., & Griest, K. 2001, ApJ, 561, 481
Franceschini, A. 1982, Ap&SS, 86, 3
Goodman, J. W. 1985, Statistical Optics (New York: Wiley)
Hodge, P., Lee, M. G., & Mateo, M. 1988, ApJ, 324, 172
Hogg, D. W. 2001, AJ, 121, 1207
Madore, B. F., & Freedman, W. L. 1998, ApJ, 492, 110
Mills, B. Y. 1984, in The Early Years of Radio Astronomy, ed. W. T. Sullivan III (Cambridge: Cambridge Univ. Press), 147
Olling, R. P., & Peterson, D. M. 2000, preprint (astro-ph/0005484)
Perryman, M. A. C., et al. 1997, A&A, 323, L49
Rajagopal, J., Allen, R. J., & Böker, T. 1999, in ASP Conf. Ser. 194, Optical and IR Interferometry from Ground and Space, ed. S. Unwin & R. Stachnik (San Francisco: ASP), 147
Ryle, M. 1959, in IAU Symp. 9, Paris Symp. on Radio Astronomy, ed. R. N. Bracewell (Stanford: Stanford Univ. Press), 475
Scheuer, P. A. G. 1957, Proc. Cambridge Philos. Soc., 53, 764
Shao, M., & Baron, R. 1999, in ASP Conf. Ser. 194, Optical and IR Interferometry from Ground and Space, ed. S. Unwin & R. Stachnik (San Francisco: ASP), 107
Shao, M., & Staelin, D. H. 1977, J. Opt. Soc. Am., 67, 81
Stanek, K. Z., & Garnavich, P. M. 1998, ApJ, 503, L131
Yoshii, Y., Ishida, K., & Stobie, R. S. 1987, AJ, 93, 323